

Development and Modeling of Ge-free Microring Avalanche Photodiode in Optical Communication Band

Yuan Yuan, Wayne V. Sorin, Di Liang, Stanley Cheung, Yiwei Peng, Mudit Jain, Zhihong Huang, Marco Fiorentino, and Raymond G. Beausoleil

Hewlett Packard Labs, Hewlett Packard Enterprise, Milpitas, CA 95035, USA

yuan.yuan@hpe.com

Abstract: A physical model was developed to unfold different optical absorption mechanisms in a Germanium-free microring avalanche photodiode. Fabricated pure-Silicon microring detector showed competitive performance to support 100 Gb/s PAM4 operations at O-band. © 2022 The Author(s)

1. Introduction

Silicon (Si) photonics technology has been widely used in photonic integrated circuits (PICs) due to its advantages of CMOS compatibility, low refractive index oxides, low cost and large wafer size. As a semiconductor with ~ 1.12 eV bandgap, Si is transparent to communication wavelengths and thus can form low-loss waveguides. But meanwhile, semiconductors with narrower bandgaps need to be integrated on Si to detect optical signals. Numerous efforts have been made to develop high-performance photodiodes (PDs) by integrating Germanium (Ge) or III-V materials on Si [1–3], however, the required monolithically or heterogeneous integration can significantly increase process complexity and cost. Nowadays, PDs based on all-Si waveguide have drawn a lot of interests. Many mechanisms have been applied to improve the sub-bandgap absorption of Si, such as defects assisted absorption (DAA), surface state absorption (SSA), internal photo-emission (IPE), and photon assisted tunneling (PAT) [4]. Recently, high responsivity Si microring resonator (MRR) based PDs have been reported [5, 6], which utilize the inherent resonance enhancement to improve the optical power in the microring waveguide. However, sub-bandgap absorption is a very weak mechanism, and the resonance enhancement cannot fully explain the high responsivity. In here, we developed a physical model to unfold different mechanisms in the MRR avalanche photodiode (APD), as evidenced by the properties of the fabricated device.

2. Device characterization

The Ge-free APD adopts a $12\ \mu\text{m}$ -radius microring structure with two-segment Si PN junctions, as shown in insert of Fig. 1(a). The two-segment MRR was originally designed for MRR modulator to more efficiently implement pulse amplitude modulation with 4 levels (PAM4) [7]. The long segment Si PN junction, which occupies $\sim 50\%$ of the MRR circumference, was biased at high reverse voltage as an APD. The measured O-band transmission spectrum of the MRR at zero bias is shown in Fig. 1(a), in which the free spectral range (FSR) is ~ 5.7 nm, the resonance dip width ($\delta\lambda$) is ~ 0.19 nm, and DC extinction ratio (ER) is ~ 9 dB. Many characteristics of the MRR then can be calculated from these measured values. The quality factor (Q) is ~ 7000 , the finesse (F) is ~ 30 , the total cavity loss coefficient (δ_c) is ~ 0.21 , the coupling loss coefficient (δ_κ) is ~ 0.14 , and the ring propagation loss coefficient (δ_r) is ~ 0.07 .

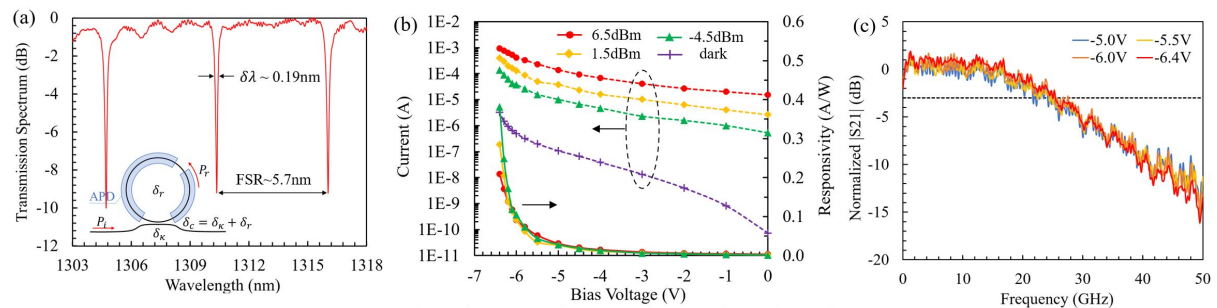


Fig. 1. Measured (a) transmission spectrum at zero bias, (b) total current, dark current, responsivity versus bias voltage, and (c) S21 response at 6.5 dBm optical power of the MRR APD.

The measured total and dark current versus bias voltage of the MRR APD is shown in Fig. 1(b), where all total current data was captured at the resonance wavelength to reach the highest value. Three optical power: 6.5 dBm, 1.5 dBm, -4.5 dBm, were applied in the bus waveguide, respectively. All total current increases with reverse bias, but it increases less with higher optical power. This phenomenon can also be clearly displayed in the measured responsivity, the highest responsivity at -4.5 dBm is ~ 0.4 A/W, which is about twice as that at 6.5 dBm. Similar

thing occurs in the APD responsivity due to the optical power dependent avalanche gain. At -6.4 V, the highest electric field of the Si PN junction is $> 5 \times 10^7$ V/m, which is sufficient to start impact ionization. Therefore, we can observe higher responsivity at lower optical power in Fig. 1(b), especially under high reverse bias.

The measured S21 responses of the MRR APD with $P_i \sim 6.5$ dBm at bias voltage of -5.0 V, -5.5 V, -6.0 V and -6.4 V are shown in Fig. 1(c). At each bias, the S21 response was measured at the wavelength with highest photocurrent. The 3 dB bandwidth slightly increases with higher reverse bias, which is ~ 24 GHz at -5.0 V and ~ 25.5 GHz at -6.4 V. This is due to the increased absorption loss at higher bias, which results in a larger ring propagation loss coefficient δ_r , and followed by a larger photon lifetime-limited bandwidth.

The measured eye diagrams of the MRR APD for 60 Gb/s non-return-to-zero (NRZ), 80 Gb/s NRZ, and 100 Gb/s PAM4 are shown in Fig. 2, respectively. Due to the instrument limitation, there is no wide bandwidth band-pass optical filter after the praseodymium-doped fiber amplifier (PDFA) and no amplifier after the MRR APD. Therefore, a high optical power, $P_i \sim 6.5$ dBm, was applied to provide detectable electric signals in the oscilloscope, and eye diagrams were averaged by 32 times to suppress the amplified spontaneous emission (ASE) noise from the EDFA. Although the APD 3 dB bandwidth at -6.4 V is ~ 25.5 GHz, the roll-off of the S21 response is not steep, which allows a 10 dB bandwidth up to ~ 40 GHz. Consequently, the open eye diagrams up to 80 Gb/s NRZ and 100 Gb/s PAM4 can be detected by the MRR APD.

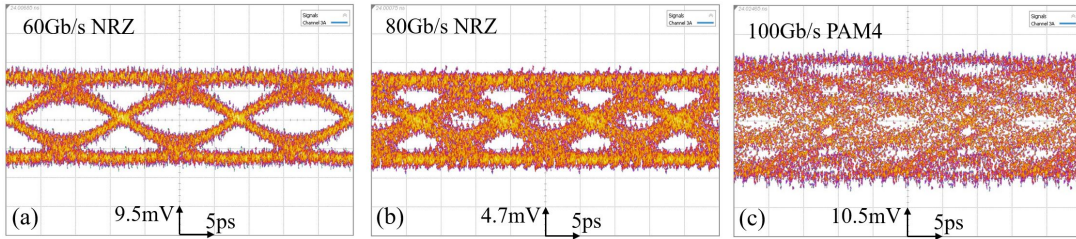


Fig. 2. Measured (a) 60 Gb/s NRZ, (b) 80 Gb/s NRZ, and (c) 100 Gb/s PAM4 eye diagrams of the MRR APD at 6.5 dBm optical power and -6.4V bias voltage.

3. Absorption model

There are four main mechanisms are included in the Si MRR APD absorption model: photon-assisted tunneling (PAT), two photon absorption (2PA), microring resonance enhancement (RE), and avalanche gain (M). PAT is a mechanism relates to the electric field across the PN junction. At 1310 nm, the photon with ~ 0.95 eV energy will injected into the Si and form a triangular potential barrier as shown in Fig. 3(a). The barrier height E_b is the energy difference between the Si bandgap and the photon energy, which is ~ 0.17 eV. While the barrier width w_b is a function of the electric field. At -6.4 V, the w_b is shorten to ~ 1.8 nm, which greatly increases the PAT probability and the PAT absorption coefficient (α_t). Additionally, because the third-order nonlinearity of Si is not zero, Si can also absorb two 0.95 eV photons simultaneously. This 2PA mechanism relates to the optical power, where the 2PA coefficient (α_2) is proportional to the optical power intensity. Consequently, PAT and 2PA constitute the photocurrent-generated absorption coefficient, α_p , expressed as

$$\alpha_p = \Gamma \cdot \alpha_t + \alpha_2 = \Gamma \cdot \alpha_t + \beta_2 \frac{RE \cdot P_i}{A}, \quad (1)$$

where Γ is the overlap factor between optical mode and depletion region in the Si PN junction, β_2 is the 2PA coefficient constant of Si, and A is the cross-sectional area of the Si ring waveguide. Such that the internal quantum efficiency of one round-trip propagation is

$$\eta \approx \frac{\alpha_p}{\alpha_{tot}} [1 - \exp(-\alpha_{tot}L)] \approx \frac{\alpha_p}{\alpha_{tot}} [1 - \exp(-\delta_r)], \quad (2)$$

where α_{tot} is the total absorption coefficient, L is the effective APD PN junction length, and δ_r has been calculated from the MRR spectrum. Besides that, microring structure can further improve the responsivity by boosting the optical power. The MRR resonance enhancement, namely the optical power ratio between the ring waveguide (P_r) and bus waveguide (P_i), can be expressed as

$$RE = \frac{P_r}{P_i} \approx \frac{4\delta_\kappa}{\delta_c^2}. \quad (3)$$

Based on the known δ_κ and δ_c , the RE of the MRR APD is ~ 12 , which means a $12 \times$ higher responsivity. Similarly, the avalanche gain further increases the responsivity by a factor of M . The Si PN junction gain value at -6.4 V can be simulated by Lumerical, which is ~ 4.5 at low optical power. As mentioned earlier, avalanche gain is a function of optical power and can generally be written as

$$M \approx -a \times 10 \log_{10}(RE \cdot P_i) + b \geq 1, \quad (4)$$

where a and b are the gain fitting parameters. For this MRR APD, the fitted optical power dependent gain curve is shown in Fig. 3(b). The fitted gain at 0.1 mW is same as the simulated gain value, ~ 4.5 . To sum up, the overall responsivity of the MRR APD can be calculated by combining these four mechanisms as

$$R = \frac{\lambda q}{h\nu} \cdot \eta \cdot RE \cdot M. \quad (5)$$

The measured responsivity versus bus waveguide optical power can verify these mechanisms. As shown in Fig. 3(c), the responsivity at -4.0 V linearly increases with optical power, which indicates that the 2PA exists in the Si MRR APD. Although the 2PA also exists at -6.4 V, the responsivity tend is quite different as shown in Fig. 3(d). The optical power dependent avalanche gain now dominates the responsivity tend. By substituting Eqs. 1-4 into Eq. 5, the calculated responsivity of the MRR APD can be displayed as the black lines in Fig. 3(c,d), which are consistent with the measured data.

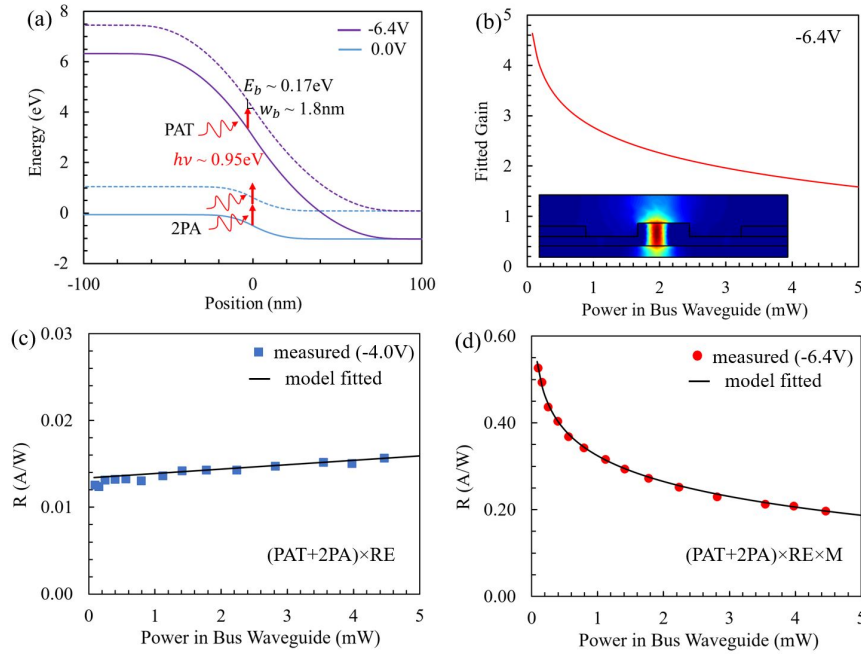


Fig. 3. (a) Simulated band diagrams of the Si PN junction at 0.0 V and -6.4 V. (b) Fitted avalanche gain and simulated electric field at -6.4 V. Measured and calculated responsivity versus bus waveguide optical power at (c) -4.0 V and (d) -6.4 V.

4. Conclusion

We developed a model to reveal the sub-bandgap absorption mechanisms inside the pure-Si MRR APD, including photon-assisted tunneling, two photon absorption, resonance enhancement, and avalanche gain. It has proven that the Ge-free MRR APD can obtain comparable responsivity to traditional PDs. The demonstrated MRR APD exhibits a responsivity up to ~ 0.5 A/W, a 3 dB bandwidth of ~ 25 GHz, and open eye diagrams of 100 Gb/s PAM4 at low voltage of -6.4 V. The absorption model provides guidance for Ge-free MRR APD design, which can further reduce the technical entrance level for CMOS foundry to develop dense Si photonics PICs.

References

1. D. Benedikovic, *et al.* "Silicon–germanium receivers for short-wave-infrared optoelectronics and communications," *Nanophotonics* **10**(3), 1059-1079 (2021).
2. Y. Yuan, *et al.* "High responsivity si-ge waveguide avalanche photodiodes enhanced by loop reflector," *IEEE J. Sel. Top. Quantum Electron.* **28** (2021).
3. K. Sun, *et al.* "40 Gbit/s waveguide photodiode using III–V on silicon heteroepitaxy," *Opt. Lett.* **45**, 2954-2956 (2021).
4. J.-B. You, *et al.* "Photon-assisted tunneling for sub-bandgap light detection in silicon pn-doped waveguides," *Opt. express* **25**, 4284-4297 (2017).
5. X. Li, *et al.* "40 gb/s all-silicon photodetector based on microring resonators," *IEEE Photonics Technol. Lett.* **27**, 729-732 (2015).
6. M. Sakib, *et al.* "A 112 gb/s all-silicon micro-ring photodetector for datacom applications," *OFC Th4A.2* (2020).
7. Y. Yuan, *et al.* "100 Gb/s PAM4 Two-Segment Silicon Microring Resonator Modulator," *IEEE IPC WG2.2* (2021).